Half-Metallic Zigzag Carbon Nanotube Dots

Oded Hod[‡,*] and Gustavo E. Scuseria

Department of Chemistry, Rice University, Houston, Texas 77005-1892. [‡]Current address: School of Chemistry, The Sackler Faculty of Exact Sciences, Tel Aviv University, Tel Aviv 69978, Israel.

ABSTRACT A comprehensive *first-principles* theoretical study of the electronic properties and half-metallic nature of finite zigzag carbon nanotubes is presented. Unlike previous reports, we find that all nanotubes studied present a spin-polarized ground state, where opposite spins are localized at the two zigzag edges in a long-range antiferromagnetic-type configuration. Relative stability analysis of the different spin states indicates that, for the shorter segments, spin-ordering should be present even at room temperature. The energy gap between the highest occupied and the lowest unoccupied molecular orbitals of the finite systems is found to be inversely proportional to the nanotube's segment lengths, suggesting a route to control their electronic properties. Similar to the case of zigzag graphene nanoribbons, half-metallic behavior is obtained under the influence of an external axial electric field.

KEYWORDS: carbon nanotubes · zigzag · finite · spin polarization · magnetic ordering · antiferromagnetic arrangement · half-metallic

Magnetism in carbon-based materials has attracted considerable scientific interest in recent years from both an experimental[1−17] and a theoretical[18−59] viewpoint. While the origin of magnetic ordering in such systems is yet to be fully understood, it has been suggested that spin polarization may arise from local structural defects,[33,36,41,55] sterically protected carbon radicals,[34] and chemical impurities.[30,40,43] A unique mechanism for spin ordering in graphene-based systems is related to the appearance of edge states.[18−29,42,46−51,53,54,56] When cutting a graphene sheet along its zigzag axis to form a narrow and elongated graphene nanoribbon (GNR), distinct electronic states appear, which are localized around the exposed edges.[60−65] These states are predicted to carry spin polarization, resulting in a well-defined magnetic ordering.[19−26,28,29,42,46−51,53,54] Due to the bipartite hexagonal structure of graphene, the electronic ground state of such zigzag graphene nanoribbons (ZZ-GNRs) is characterized by a long-range antiferromagnetic-type (AFM) spin ordering, where the edge states located at the two zigzag edges of the ribbon have opposite spins.[66] Under the influence of an external electric field, these systems have been predicted to become half-metallic with one spin channel being semiconducting and the other metallic,[46,48] thus acting as perfect spin filters with important implications to the field of spintronics. Furthermore, this behavior has been shown to be preserved for finite graphene nanoribbons, where the zigzag edge may be as short as a few repeating units.[49−51,53,54]

Similar to graphene nanoribbons, it has recently been suggested that spin ordering may occur on the zigzag edges of hydrogen-terminated finite-sized carbon nanotubes (CNTs).[32,37] On the basis of density functional theory (DFT) calculations within the local spin density approximation (LSDA), it was predicted that the electronic ground state of these systems strongly depends on their circumferential dimension ranging from AFM to ferromagnetic-type (FM) ordering, where both edges of the nanotube bear spins of the same flavor. This conclusion is in striking difference from the case of ZZ-GNRs, where the ground electronic state was found to have an AFM spin ordering regardless of the dimensions of the ribbon.[19−26,28,29,42,46−51,53,54]

Interestingly, contradicting results have been reported in the literature,[33] indicating that the ground state of unpassivated zigzag CNTs has a low-spin AFM ordering even for nanotubes that have earlier been considered to present a high-spin ferromagnetic-type ordered ground state.[32] This is further supported by a recent study discussing both the AFM-type ground state and the half-metallic nature of hydrogen-passivated finite (14,0) zigzag CNT segments.[59]

*Address correspondence to odedhod@tau.ac.il.

Received for review June 27, 2008 and accepted September 30, 2008.

Published online October 16, 2008.
10.1021/nn8004069 CCC: $40.75

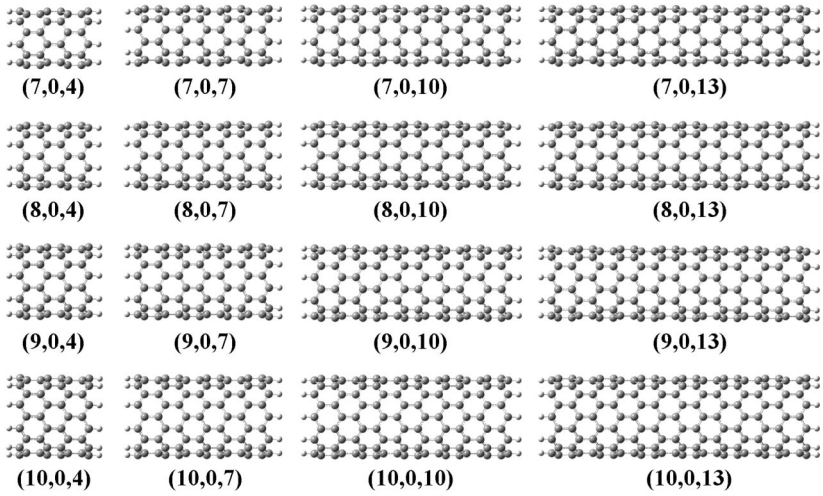

Figure 1. Four sets of CNTs studied. The notation (*N*, *M*, *L*) indicates a finite segment of a (*N*, *M*) CNT with *L* zigzag carbon rings along its principal axis.

In light of the considerable progress that has been made in the synthesis and fabrication of ultrashort[67−71] and open ended[72] CNTs and ultranarrow GNRs,[73−76] it is desirable to obtain a full understanding of their electronic properties. Such understanding may prove important in future applications of these molecules in nanoelectronic and nanospintronic devices.

It is the purpose of the present paper to present a comprehensive investigation of spin polarization in hydrogen-passivated finite zigzag CNTs. Unlike previous reports on these systems,[32,37] we find that all zigzag CNTs studied present an antiferromagnetic-type ordered ground state, regardless of their diameter and length. Furthermore, as is the case with infinitely long[46−48] and finite[54] GNRs, the application of an external axial electric field results in half-metallic behavior.

RESULTS AND DISCUSSION

We study a set of 16 finite segments of the (7,0), (8,0), (9,0), and (10,0) zigzag CNTs (see Figure 1). For each CNT, four segments of 0.93, 1.56, 2.20, and 2.84 nm in length are considered. All nanotubes considered are hydrogen terminated; that is, each carbon edge atom is passivated with a single hydrogen atom. We label the CNTs with (*N*, *M*, *L*), where (*N*, *M*) is the infinite CNT from which the relevant finite segment is derived and *L* is the number of zigzag carbon rings stacked together to form the finite CNT (see Figure 1). This set of nanotubes includes all those previously predicted to present a long-range ferromagnetic-type ordered ground state.[32]

We start by performing ground state calculations for the full set of 16 finite CNTs studied. In Figure 2, spin density maps of the ground state of four representative CNT segments are presented. In contradiction with previously reported LSDA results,[32,37] which predict the (8, 0) CNT derivatives to have an AFM ground state and the (7, 0) and (10, 0) nanotube segments to have a ferromagnetically ordered ground state, our calculations, using the HSE06 screened hybrid density functional (see the Methods and Computational Details section below), indicate that all CNTs studied have an antiferromagnetically ordered ground state, with a total spin vector projection of $m_s = 0$ and a spatially resolved spin density. Similar to the case of finite GNRs,[49,54] one zigzag edge of the CNTs' segments has a high density of spin α electrons (blue color in Figure 2) while the other edge is rich in spin β electrons (red color in the figure).

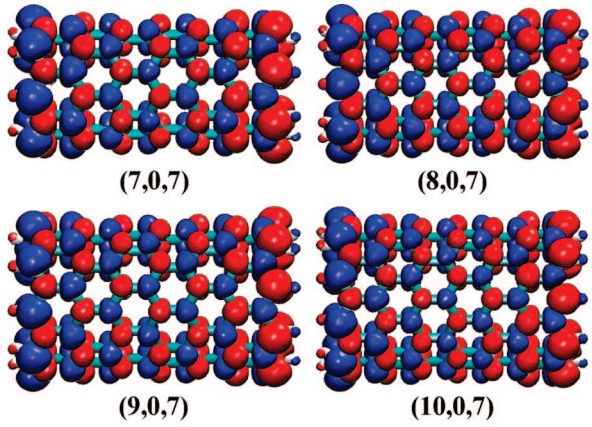

Figure 2. Antiferromagnetic-type ground state spin density maps of the (7,0,7) (upper left panel), (8,0,7) (upper right panel), (9,0,7) (lower left panel), (10,0,7) (lower right panel) finite zigzag CNTs as obtained using the HSE06 functional with the 6-31G basis set. Red and blue isosurfaces indicate the two spin flavors with an isovalue of 0.0015 a_0^{-3}.**

To understand the origin of this discrepancy between previous predictions obtained using the local density functional approximation and the current screened-hybrid functional results, we have repeated the calculations using the LSDA functional[77] and the same atomic basis set. We have found that for the (7, 0, 7) and (7, 0, 10) systems the LSDA functional does predict a ferromagnetically ordered ground state. Nevertheless, this state is only 5 meV below the antiferromagnetically ordered state. For the rest of the systems considered, an AFM ground state has been found.

We attribute these differences to the self-interaction error appearing in the LSDA functional, which tends to considerably overestimate electron delocalization.[78,79] Since some of the most important physical characteristics of the systems under consideration relate to pronounced localized edge states, care should be taken when using the LSDA functional to capture the correct energetic ordering of the different spin-polarized states. As discussed in the Methods and Computational Details section, the inclusion of Hartree−Fock exchange within hybrid functionals considerably reduces the delocalization error and thus makes them more appropriate to treat scenarios where electron localization plays

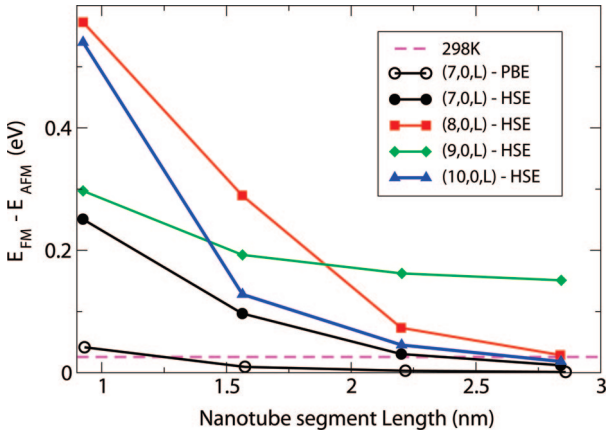

Figure 3. Energy differences between the antiferromagnetic ground state and the above lying higher spin multiplicity ferromagnetic state for the four sets of CNTs segments studied, as calculated by the HSE06 (filled marks) and the PBE (empty marks) functionals. k_BT at room temperature is indicated by the dashed magenta line.

an important role in determining the electronic structure of the system.[80−84]

To quantify our findings, we study the stability of the antiferromagnetically ordered ground state with respect to the above lying ferromagnetically ordered spin state. In Figure 3, the energy differences between the antiferromagnetic ground state and the first higher spin multiplicity state are presented for the four sets of nanotube segments studied. We indicate k_BT (k_B being Boltzmann's constant) at room temperature ($T = 298$ K) by the dashed magenta line in the figure. For the (7, 0, L) and (9, 0, L) systems, we find the $m_s = 2$ state to be the above lying ferromagnetic state. For the (10, 0, L) segments, the first higher spin multiplicity state has $m_s = 3$. In the case of the (8, 0, L) segments, the higher spin multiplicity state changes from $m_s = 1$ for $L = 4$ to $m_s = 3$ for $L = 7$, 10, and 13. As can be seen, the AFM ground state of the shorter CNT segments studied is considerably more stable than the above lying higher spin state and is expected to be detectable at room temperature. Like in the case of GNRs,[46] the energy difference between the ground state and the above lying higher spin state decreases monotonically with increasing CNT length, up to a point where the differences become lower than room temperature. Interestingly, we find that for the (9, 0) segments, which in the limit of infinite length become metallic, the decay rate of the energy difference between the AFM ground state and the above lying FM state is slower than that of the other semiconducting tubes studied. Nevertheless, even for this system, an exponential fit of the decay curve suggests that at a length of 8 nm the energy difference is below room temperature.

For completeness, we have performed test calculations using the Perdew−Burke−Ernzerhof (PBE) semilocal functional[77,85] and the same atomic basis set (see Methods and Computational Details section) for the (7, 0) subset of CNT segments. The results of these calculations are indicated by the empty circle marks in Figure 3. We find that, similar to the HSE06 functional, the PBE results predict an AFM-type arrangement for the ground state of all (7, 0) CNT segments studied. Nevertheless, the energy differences between the AFM-type ground state of each segment and the above lying $m_s = 2$ state are considerably smaller than those obtained by the HSE06 functional.

Figure 4 shows the energy difference between the AFM ground state and the $m_s = 0$ (closed shell), $m_s = 1$, 2, 3, and 4 electronic states of the (10, 0, L) CNT segments. The nonmagnetic state is found to be considerably higher in energy compared to all high spin multiplicity states presented in the figure (except for the $m_s = 4$ state of the shortest CNT segment). This is in agreement with the case of GNRs[46,54] and suggests that even at room temperature short segments of CNTs are expected to present magnetic properties. It should be mentioned that for the $m_s = 1$ and 2 cases, as the length of the CNT is increased, the spin arrangement changes from a FM-type to a mixed configuration where both spin polarizations appear on the same edge of the CNT. This, as well, was previously observed in the case of finite GNRs.[54]

Before discussing the effect of an electric field on the electronic properties of finite CNTs, it is essential to study their ground state characteristics in the absence of external perturbations. The length dependence of the HOMO−LUMO (highest occupied molecular orbital and lowest unoccupied molecular orbital, respectively) gap would be the most important parameter to address. In Figure 5, this energy gap as a function of the length of the CNT segments is presented for the four subsets of nanotubes considered. All studied finite zigzag CNT segments have sizable HOMO−LUMO gaps, including the (9, 0, L) series, which in the limit of $L \rightarrow \infty$

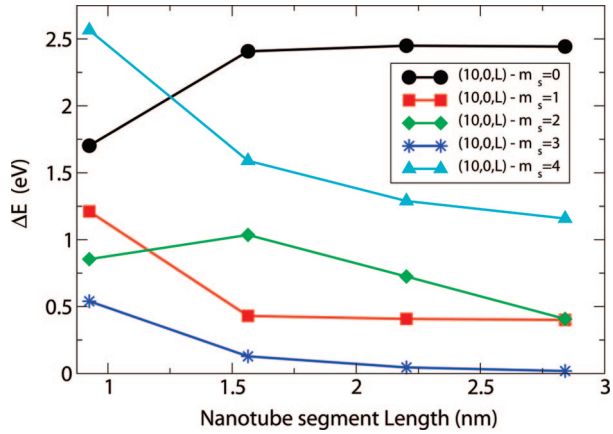

Figure 4. Energy differences between the antiferromagnetic ground state and the closed shell (black circles), $m_s = 1$ (red squares), $m_s = 2$ (green diamonds), $m_s = 3$ (blue stars), and $m_s = 4$ (cyan triangles) states for the (10, 0, L) CNT segments, as calculated by the HSE06 functional.

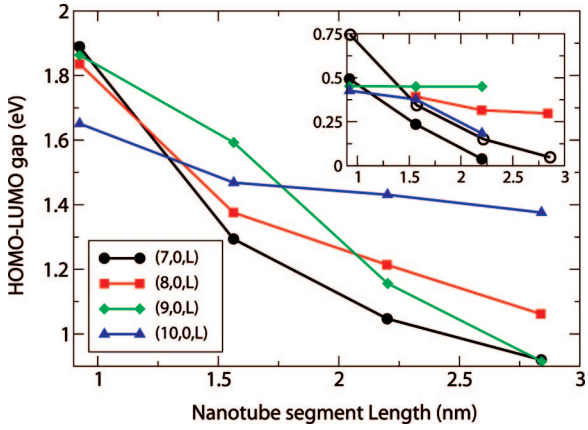

Figure 5. HOMO−LUMO gap values as a function of CNT segment length for the four sets of CNTs studied as calculated by the HSE06 functional. Inset: HOMO−LUMO gap values as a function of CNT segment length as calculated at the LSDA (filled marks) and PBE (empty marks for the (7, 0, *L*) segments) level of theory.

is expected to become metallic. The HOMO−LUMO gap is inversely proportional to the length of the CNT segments for all nanotubes studied, and its value strongly depends on the length, changing by more than 0.8 eV for lengths in the range of 0.9 and 2.8 nm. This suggest that careful tailoring of the nanotube length can be used as a sensitive control parameter over its electronic properties.[86] For comparison purposes, we present, in the inset of Figure 5, the HOMO−LUMO gap values of the AFM state as obtained by the LSDA and the PBE functionals. Even though, in some cases, the LSDA calculations fail to predict the correct energetic ordering of the different spin states, the HOMO−LUMO gap behavior presents a trend similar to that obtained by the screened hybrid functional. As expected, the values of the HOMO−LUMO gaps obtained by the hybrid functional are considerably higher than those obtained by the LSDA approximation. The PBE predictions resemble the LSDA results, although the absolute values of the HOMO−LUMO gaps obtained with the semilocal functional are somewhat higher than those predicted by the strictly local approximation.

We now turn to check whether the similarity between finite zigzag CNTs and finite GNRs extends also to the case of half-metallic behavior under the influence of an external electric field.[46,54] In Figure 6, we present the spin-polarized HOMO−LUMO gap dependence on an external electric field applied parallel to the main axis of the nanotubes (perpendicular to the zigzag edges) for four representative finite zigzag CNTs. In agreement with previous calculations,[46,48,54] the α and β gaps are degenerate in the absence of an external field. Upon application of the field, electrons having one spin experience an increase in the HOMO−LUMO gap while the opposite spin flavor experiences a decrease in the gap. This gap splitting continues up to a point, where one spin channel presents a vanishing gap, thus creating a half-metallic state or a perfect spin filter. At this point, due to the increased mobility of the metallic electrons, further increase in the external field results in spin transfer between both edges, thus reducing the total spin polarization and the energy gap splitting (this can be clearly seen on the upper left panel of Figure 6). All four representative structures present the same features described above. The main differences observed are in the zero field HOMO−LUMO gap and the onset field for the appearance of the half-metallic state. Nevertheless, they all predict a half-metallic state at an appropriate electric field strength.

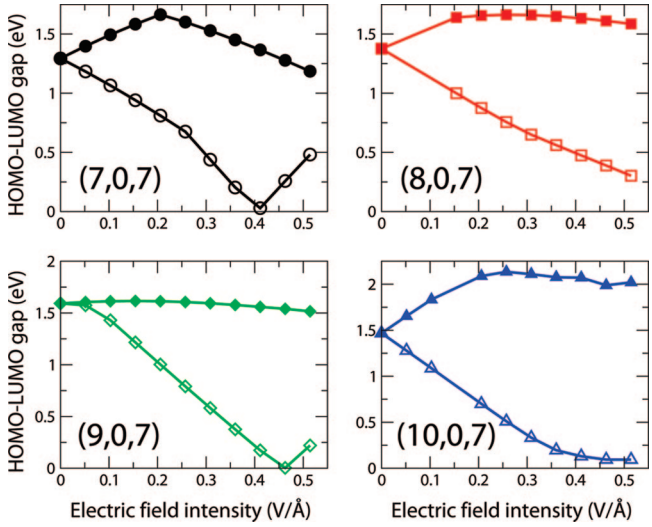

Figure 6. Spin-polarized HOMO−LUMO gap dependence on the strength of an external axial electric field for the (7, 0, 7) (upper left panel), (8, 0, 7) (upper right panel), (9, 0, 7) (lower left panel), and (10, 0, 7) (lower right panel) finite zigzag CNTs as calculated by the HSE06 functional. Fixed geometries of the relaxed structures in the absence of the external field were used. Full and open marks are the α and β spin gaps, respectively.

CONCLUSIONS

To summarize, intrigued by reports of contradicting results regarding the ground state properties of finite zigzag carbon nanotubes, we performed a comprehensive study of the electronic character of a representative set of 16 CNT segments. Unlike previously reported results, we found that all finite zigzag CNTs possess a spin-polarized ground state with a long-range antiferromagnetic-type spin ordering. This state is characterized by high spin density of opposite spins located at the two zigzag edges of the molecule. Our HSE06 results predict the antiferromagnetic-type ordering to be considerably stable than the higher spin multiplicity states and the nonmagnetic closed shell state, suggesting that their spin polarization is detectable at room temperature. The HOMO−LUMO gap was found to be inversely proportional to the length of the zigzag CNT segment. The high sensitivity of the gap to changes in the length of the CNT segment suggests a way to control the electronic properties of such systems. Similar to the case of zigzag GNRs, the half-

metallic nature of finite zigzag CNTs under an external in-plane electric field was verified. Due to the recent success of the HSE06 functional in predicting the electronic properties of GNRs and CNTs of different nature and dimensions, we are confident about the reliability of the predictions presented here.

METHODS AND COMPUTATIONAL DETAILS

All of the calculations presented in this work were carried out using the development version of the Gaussian suite of programs.[87] Unless otherwise stated, spin-polarized ground state calculations[88] were performed using the screened exchange hybrid density functional of Heyd, Scuseria, and Ernzerhof (HSE06),[77,89−91] which has been tested on a wide variety of materials and has been shown to accurately reproduce experimental band gaps[92−94] and first and second optical excitation energies in metallic and semiconducting single-walled CNTs.[95,96] The inclusion of short-range exact-exchange in the HSE06 functional makes it suitable to treat electronic localization effects,[80−84] which are known to be important in these types of materials.[18−29,42,46−49,54,62−65] This is further supported by the good agreement, which was recently obtained, between predicted band gaps[97] of narrow graphene nanoribbons and measured values.[73−75] To obtain a reliable ordering of the different magnetization states, we find it important to relax the geometry of the finite CNTs for each spin polarization. Therefore, unless otherwise stated, all reported electronic properties are given for fully optimized structures using the double-ζ polarized 6-31G** Gaussian basis set.[98]

As stated above, sample calculations using local and semilocal functionals were performed for comparison purposes. Interestingly, when using the local spin density approximation, we encountered considerable convergence problems. For many of the systems, we have found it necessary to restart the self-consistent field (SCF) procedure with a predesigned initial guess in order to achieve convergence to the appropriate spin state. In some cases, even this approach did not lead to a converged result.

It should be noted that, since our calculations are performed within a single determinantal framework, we can determine only the total spin vector projection along a given axis, m_s, and not the total spin. This is standard in unrestricted Kohn−Sham theory.

Acknowledgment. This work was supported by NSF CHE-0807194 and the Welch Foundation (C-0036). Calculations were performed in part on the Rice Terascale Cluster funded by NSF under Grant EIA-0216467, Intel, and HP and on the Shared University Grid at Rice funded by NSF under Grant EIA-0216467, and a partnership between Rice University, Sun Microsystems, and Sigma Solutions, Inc. O.H. would like to thank the generous financial support of the Rothschild and Fulbright foundations.

REFERENCES AND NOTES

1. Shibayama, Y.; Sato, H.; Enoki, T.; Endo, M. Disordered Magnetism at the Metal-Insulator Threshold in Nano-Graphite-Based Carbon Materials. *Phys. Rev. Lett.* **2000**, *84*, 1744–1747.
2. Prasad, B. L. V.; Sato, H.; Enoki, T.; Hishiyama, Y.; Kaburagi, Y.; Rao, A. M.; Eklund, P. C.; Oshida, K.; Endo, M. Heat-Treatment Effect on the Nanosized Graphite p-Electron System During Diamond to Graphite Conversion. *Phys. Rev. B* **2000**, *62*, 11209–11218.
3. Kopelevich, Y.; Esquinazi, P.; Torres, J. H. S.; Moehlecke, S. Ferromagnetic- and Superconducting-Like Behavior of Graphite. *J. Low Temp. Phys.* **2000**, *119*, 691–702.
4. Makarova, T. L.; Sundqvist, B.; Höhne, R.; Esquinazi, P.; Kopelevich, Y.; Scharff, P.; Davydov, V. A.; Kashevarova, L. S.; Rakhmanina, A. V. Magnetic Carbon. *Nature* **2001**, *413*, 716–718.
5. Takai, K.; Sato, H.; Enoki, T.; Yoshida, N.; Okino, F.; Touhara, H.; Endo, M. Effect of Fluorination on Nano-Sized π-Electron Systems. *J. Phys. Soc. Jpn.* **2001**, *70*, 175–185.
6. Coey, J. M. D.; Venkatesan, M.; Fitzgerald, C. B.; Douvalis, A. P.; Sanders, I. S. Ferromagnetism of a Graphite Nodule from the Canyon Diablo Meteorite. *Nature* **2002**, *420*, 156–159.
7. Esquinazi, P.; Setzer, A.; Höhne, R.; Semmelhack, C.; Kopelevich, Y.; Spemann, D.; Butz, T.; Kohlstrunk, B.; Lösche, M. Ferromagnetism in Oriented Graphite Samples. *Phys. Rev. B* **2002**, *66*, 024429-1–024429-10.
8. Wood, R. A.; Lewis, M. H.; Lees, M. R.; Bennington, S. M.; Cain, M. G.; Kitamura, N. Ferromagnetic Fullerene. *J. Phys.: Condens. Matter* **2002**, *14*, L385–L391.
9. Höhne, R.; Esquinazi, P. Can Carbon Be Ferromagnetic. *Adv. Mater.* **2002**, *14*, 753–756.
10. Esquinazi, P.; Spemann, D.; Höhne, R.; Setzer, A.; Han, K.-H.; Butz, T. Induced Magnetic Ordering by Proton Irradiation in Graphite. *Phys. Rev. Lett.* **2003**, *91*, 227201-1–227201-4.
11. Makarova, T. L. Magnetic Properties of Carbon Structures. *Semiconductors* **2004**, *38*, 615–638.
12. Esquinazi, P.; Han, K. H.; Houmlhne, R.; Spemann, D.; Setzer, A.; Butz, T. Examples of Room-Temperature Magnetic Ordering in Carbon-Based Structures. *Phase Transitions* **2005**, *78*, 155–171.
13. Mombrú, A. W.; Pardo, H.; Faccio, R.; de Lima, O. F.; Leite, E. R.; Zanelatto, G.; Lanfredi, A. J. C.; Cardoso, C. A.; Araújo-Moreira, F. M. Multilevel Ferromagnetic Behavior of Room-Temperature Bulk Magnetic Graphite. *Phys. Rev. B* **2005**, *71*, 100404(R)-1100404(R)-4.
14. Makarova, T.; Palacio, F. *Carbon Based Magnetism: An Overview of the Magnetism of Metal Free Carbon-based Compounds and Materials*; Elsevier: Amsterdam, 2006.
15. Ohldag, H.; Tyliszczak, T.; Höhne, R.; Spemann, D.; Esquinazi, P.; Ungureanu, M.; Butz, T. π-Electron Ferromagnetism in Metal-Free Carbon Probed by Soft X-Ray Dichroism. *Phys. Rev. Lett.* **2007**, *98*, 187204-1–187204-4.
16. Tombros, N.; Jozsa, C.; Popinciuc, M.; Jonkman, H. T.; van Wees, B. J. Electronic Spin Transport and Spin Precession in Single Graphene Layers at Room Temperature. *Nature* **2007**, *448*, 571–574.
17. Likodimos, V.; Glenis, S.; Guskos, N.; Lin, C. L. Antiferromagnetic Behavior in Single-Wall Carbon Nanotubes. *Phys. Rev. B* **2007**, *76*, 075420-1–075420-5.
18. Kobayashi, K. Electronic Structure of a Stepped Graphite Surface. *Phys. Rev. B* **1993**, *48*, 1757–1760.
19. Klein, D. J. Graphitic Polymer Strips with Edge States. *Chem. Phys. Lett.* **1994**, *217*, 261–265.
20. Fujita, M.; Wakabayashi, K.; Nakada, K.; Kusakabe, K. Peculiar Localized State at Zigzag Graphite Edge. *J. Phys. Soc. Jpn.* **1996**, *65*, 1920–1923.
21. Nakada, K.; Fujita, M.; Dresselhaus, G.; Dresselhaus, M. S. Edge State in Graphene Ribbons: Nanometer Size Effect and Edge Shape Dependence. *Phys. Rev. B* **1996**, *54*, 17954–17961.
22. Wakabayashi, K.; Sigrist, M.; Fujita, M. SpinWave Mode of Edge-Localized Magnetic States in Nanographite Zigzag Ribbons. *J. Phys. Soc. Jpn.* **1998**, *67*, 2089–2093.
23. Nakada, K.; Igami, M.; Fujita, M. Electron-Electron Interaction in Nanographite Ribbons. *J. Phys. Soc. Jpn.* **1998**, *67*, 2388–2394.
24. Wakabayashi, K.; Fujita, M.; Ajiki, H.; Sigrist, M. Electronic and Magnetic Properties of Nanographite Ribbons. *Phys. Rev. B* **1999**, *59*, 8271–8282.
25. Miyamoto, Y.; Nakada, K.; Fujita, M. First-Principles Study of Edge States of H-Terminated Graphitic Ribbons. *Phys. Rev. B* **1999**, *59*, 9858–9861.
26. Kawai, T.; Miyamoto, Y.; Sugino, O.; Koga, Y. Graphitic Ribbons without Hydrogen-Termination: Electronic

Structures and Stabilities. *Phys. Rev. B* **2000**, *62*, R16349–R16352.
27. Okada, S.; Oshiyama, A. Magnetic Ordering in Hexagonally Bonded Sheets with First-Row Elements. *Phys. Rev. Lett.* **2001**, *87*, 146803-1–146803-4.
28. Kusakabe, K.; Maruyama, M. Magnetic Nanographite. *Phys. Rev. B* **2003**, *67*, 092406-1–092406-4.
29. Yamashiro, A.; Shimoi, Y.; Harigaya, K.; Wakabayashi, K. Spin- and Charge-Polarized States in Nanographene Ribbons with Zigzag Edges. *Phys. Rev. B* **2003**, *68*, 193410-1–193410-4.
30. Lehtinen, P. O.; Foster, A. S.; Ayuela, A.; Krasheninnikov, A.; Nordlund, K.; Nieminen, R. M. Magnetic Properties and Diffusion of Adatoms on a Graphene Sheet. *Phys. Rev. Lett.* **2003**, *91*, 017202-1–017202-4.
31. Andriotis, A. N.; Menon, M.; Sheetz, R. M.; Chernozatonskii, L. Magnetic Properties of C60 Polymers. *Phys. Rev. Lett.* **2003**, *90*, 026801-1–026801-4.
32. Okada, S.; Oshiyama, A. Nanometer-Scale Ferromagnet: Carbon Nanotubes with Finite Length. *J. Phys. Soc. Jpn.* **2003**, *72*, 1510–1515.
33. Kim, Y.-H.; Choi, J.; Chang, K. J.; Tománek, D. Defective Fullerenes and Nanotubes as Molecular Magnets: An *Ab Initio* Study. *Phys. Rev. B* **2003**, *68*, 125420-1–125420-4.
34. Park, N.; Yoon, M.; Berber, S.; Ihm, J.; Osawa, E.; Tománek, D. Magnetism in All-Carbon Nanostructures with Negative Gaussian Curvature. *Phys. Rev. Lett.* **2003**, *91*, 237204-1–237204-4.
35. Hikihara, T.; Hu, X.; Lin, H.-H.; Mou, C.-Y. Ground-State Properties of Nanographite Systems with Zigzag Edges. *Phys. Rev. B* **2003**, *68*, 035432-1–035432-9.
36. Ma, Y.; Lehtinen, P. O.; Foster, A. S.; Nieminen, R. M. Magnetic Properties of Vacancies in Graphene and Single-Walled Carbon Nanotubes. *New J. Phys.* **2004**, *6*, 68-1–68-15.
37. Higuchi, Y.; Kusakabe, K.; Suzuki, N.; Tsuneyuki, S.; Yamauchi, J.; Akagi, K.; Yoshimoto, Y. Nanotube-Based Molecular Magnets with Spin-Polarized Edge States. *J. Phys.: Condens. Matter* **2004**, *16*, S5689–S5692.
38. Kusakabe, K.; Maruyama, M.; Tsuneyuki, S.; Akagi, K.; Yoshimoto, Y.; Yamauchi, J. Indication of Flat-Band Magnetism in Theoretically Designed Nanographite with Modified Zigzag Edges. *J. Magn. Magn. Mater.* **2004**, *272−276*, E737–E738.
39. Ryu, S.; Hatsugai, Y. Zero-Energy Edge States and Chiral Symmetry Breaking at Edges of Graphite Sheets. *Physica E* **2004**, *22*, 679–683.
40. Lehtinen, P. O.; Foster, A. S.; Ayuela, A.; Vehvilinen, T. T.; Nieminen, R. M. Structure and Magnetic Properties of Adatoms on Carbon Nanotubes. *Phys. Rev. B* **2004**, *69*, 155422-1–155422-5.
41. Lehtinen, P. O.; Foster, A. S.; Ma, Y.; Krasheninnikov, A. V.; Nieminen, R. M. Irradiation-Induced Magnetism in Graphite: A Density Functional Study. *Phys. Rev. Lett.* **2004**, *93*, 187202-1–187202-4.
42. Lee, H.; Son, Y.-W.; Park, N.; Han, S.; Yu, J. Magnetic Ordering at the Edges of Graphitic Fragments: Magnetic Tail Interactions between the Edge-Localized States. *Phys. Rev. B* **2005**, *72*, 174431-1–174431-8.
43. Ma, Y.; Lehtinen, P. O.; Foster, A. S.; Nieminen, R. M. Hydrogen-Induced Magnetism in Carbon Nanotubes. *Phys. Rev. B* **2005**, *72*, 085451-1–085451-6.
44. Chen, R. B.; Chang, C. P.; Hwang, J. S.; Chuu, D. S.; Lin, M. F. Magnetization of Finite Carbon Nanotubes. *J. Phys. Soc. Jpn.* **2005**, *74*, 1404–1407.
45. Hod, O.; Rabani, E.; Baer, R. Magnetoresistance Devices Based on Single Walled Carbon Nanotubes. *J. Chem. Phys.* **2005**, *123*, 051103-1–051103-4.
46. Son, Y.-W.; Cohen, M. L.; Louie, S. G. Half-Metallic Graphene Nanoribbons. *Nature* **2006**, *444*, 347–349.
47. Son, Y.-W.; Cohen, M. L.; Louie, S. G. Energy Gaps in Graphene Nanoribbons. *Phys. Rev. Lett.* **2006**, *97*, 216803-1–216803-4.
48. Hod, O.; Barone, V.; Peralta, J. E.; Scuseria, G. E. Enhanced Half-Metallicity in Edge-Oxidized Zigzag Graphene Nanoribbons. *Nano Lett.* **2007**, *7*, 2295–2299.
49. Hod, O.; Peralta, J. E.; Scuseria, G. E. Edge Effects in Finite Elongated Graphene Nanoribbons. *Phys. Rev. B* **2007**, *76*, 233401-1–233401-4.
50. Fernndez-Rossier, J.; Palacios, J. J. Magnetism in Graphene Nanoislands. *Phys. Rev. Lett.* **2007**, *99*, 177204-1–177204-4.
51. Ezawa, M. Metallic Graphene Nanodisks: Electronic and Magnetic Properties. *Phys. Rev. B* **2007**, *76*, 245415-1–245415-6.
52. Gunlycke, D.; Li, J.; Mintmire, J. W.; White, C. T. Altering Low-Bias Transport in Zigzag-Edge Graphene Nanostrips with Edge Chemistry. *Appl. Phys. Lett.* **2007**, *91*, 112108-1–112108-3.
53. Ezawa, M. Graphene Nanoribbon and Graphene Nanodisk. *Physica E* **2008**, *40*, 1421–1423.
54. Hod, O.; Barone, V.; Scuseria, G. E. Half-Metallic Graphene Nanodots: A Comprehensive First-Principles Theoretical Study. *Phys. Rev. B* **2008**, *77*, 035411-1–035411-6.
55. Pisani, L.; Montanari, B.; Harrison, N. M. A Defective Graphene Phase Predicted to be a Room Temperature Ferromagnetic Semiconductor. *New J. Phys.* **2008**, *10*, 033002-1–033022-9.
56. Kudin, K. N. Zigzag Graphene Nanoribbons with Saturated Edges. *ACS Nano* **2008**, *2*, 516–522.
57. Sebastiani, D.; Kudin, K. N. Electronic Response Properties of Carbon Nanotubes in Magnetic Fields. *ACS Nano* **2008**, *2*, 661–668.
58. Hu, S.; Li, Z.; Zeng, X. C.; Yang, J. Electronic Structures of Defective Boron Nitride Nanotubes under Transverse Electric Fields. *J. Phys. Chem. C* **2008**, *112*, 8424–8428.
59. Mañanes, A.; Duque, F.; Ayuela, A.; López, M. J.; Alonso, J. A. Half-Metallic Finite Zigzag Single-Walled Carbon Nanotubes from First Principles. *Phys. Rev. B* **2008**, *78*, 035432-1–035432-10.
60. Giunta, P. L.; Kelty, S. P. Direct Observation of Graphite Layer Edge States by Scanning Tunneling Microscopy. *J. Chem. Phys.* **2001**, *114*, 1807–1812.
61. Klusek, Z.; Kozlowski, W.; Waqar, Z.; Datta, S.; Burnell-Gray, J. S.; Makarenko, I.; Gall, N. R.; Rutkov, E. V.; Tontegode, A. Y.; Titkov, A. N. Local Electronic Edge States of Graphene Layer Deposited on Ir(111) Surface Studied by STM/CITS. *Appl. Surf. Sci.* **2005**, *252*, 1221–1227.
62. Kobayashi, Y.; ichi Fukui, K.; Enoki, T.; Kusakabe, K.; Kaburagi, Y. Observation of Zigzag and Armchair Edges of Graphite using Scanning Tunneling Microscopy and Spectroscopy. *Phys. Rev. B* **2005**, *71*, 193406-1–193406-4.
63. Niimi, Y.; Matsui, T.; Kambara, H.; Tagami, K.; Tsukada, M.; Fukuyama, H. Scanning Tunneling Microscopy and Spectroscopy Studies of Graphite Edges. *Appl. Surf. Sci.* **2005**, *241*, 43–48.
64. Niimi, Y.; Matsui, T.; Kambara, H.; Tagami, K.; Tsukada, M.; Fukuyama, H. Scanning Tunneling Microscopy and Spectroscopy of the Electronic Local Density of States of Graphite Surfaces near Monoatomic Step Edges. *Phys. Rev. B* **2006**, *73*, 085421-1–085421-8.
65. Kobayashi, Y.; Fukui, K. I.; Enoki, T.; Kusakabe, K. Edge State on Hydrogen-Terminated Graphite Edges Investigated by Scanning Tunneling Microscopy. *Phys. Rev. B* **2006**, *73*, 125415-1–125415-8.
66. This should not be confused with the term antiferromagnetic ordering commonly used in solid state physics to describe antiparallel spin alignments on adjacent lattice sites.
67. Gu, Z.; Peng, H.; Hauge, R. H.; Smalley, R. E.; Margrave, J. L. Cutting Single-Wall Carbon Nanotubes through Fluorination. *Nano Lett.* **2002**, *2*, 1009–1013.
68. Nakamura, E.; Tahara, K.; Matsuo, Y.; Sawamura, M. Synthesis, Structure, and Aromaticity of a Hoop-Shaped Cyclic Benzenoid [10]Cyclophenacene. *J. Am. Chem. Soc.* **2003**, *125*, 2834–2835.
69. Javey, A.; Qi, P.; Wang, Q.; Dai, H. Ten- to 50-nm-long Quasi-Ballistic Carbon Nanotube Devices Obtained

without Complex Lithography. *Proc. Natl. Acad. Sci. U.S.A.* **2004**, *101*, 13408–13410.
70. Chen, Z.; Kobashi, K.; Rauwald, U.; Booker, R.; Fan, H.; Hwang, W.-F.; Tour, J. M. Soluble Ultra-Short Single-Walled Carbon Nanotubes. *J. Am. Chem. Soc.* **2006**, *128*, 10568–10571.
71. Chen, Z.; Ziegler, K. J.; Shaver, J.; Hauge, R. H.; Smalley, R. E. Cutting of Single-Walled Carbon Nanotubes by Ozonolysis. *J. Phys. Chem. B* **2006**, *110*, 11624–11627.
72. Ajayan, P. M.; Ebbesen, T. W.; Ichihashi, T.; Iijima, S.; Tanigaki, K.; Hiura, H. Opening Carbon Nanotubes with Oxygen and Implications for Filling. *Nature* **1993**, *362*, 522–525.
73. Han, M. Y.; Özyilmaz, B.; Zhang, Y.; Kim, P. Energy Band Gap Engineering of Graphene Nanoribbons. *Phys. Rev. Lett.* **2007**, *98*, 206805-1–206805-4.
74. Chen, Z.; Lin, Y.-M.; Rooks, M. J.; Avouris, P. Graphene Nano-Ribbon Electronics. *Physica E* **2007**, *40*, 228–232.
75. Li, X.; Wang, X.; Zhang, L.; Lee, S.; Dai, H. Chemically Derived, Ultrasmooth Graphene Nanoribbon Semiconductors. *Science* **2008**, *319*, 1229–1232.
76. Wang, X.; Ouyang, Y.; Li, X.; Wang, H.; Guo, J.; Dai, H. Room-Temperature All-Semiconducting Sub-10-nm Graphene Nanoribbon Field-Effect Transistors. *Phys. Rev. Lett.* **2008**, *100*, 206803-1–206803-4.
77. The local spin density, gradient corrected, and screened hybrid approximations are obtained using the SVWN5, PBEPBE, and HSE1PBE keywords in the development version of Gaussian, respectively.
78. Ruzsinszky, A.; Perdew, J. P.; Csonka, G. I.; Vydrov, O. A.; Scuseria, G. E. Spurious Fractional Charge on Dissociated Atoms: Pervasive and Resilient Self-Interaction Error of Common Density Functionals. *J. Chem. Phys.* **2006**, *125*, 194112-1–194112-8.
79. Mori-Sánchez, P.; Cohen, A. J.; Yang, W. Many-Electron Self-Interaction Error in Approximate Density Functionals. *J. Chem. Phys.* **2006**, *125*, 201102-1–201102-4.
80. Kudin, K. N.; Scuseria, G. E.; Martin, R. L. Hybrid Density Functional Theory and the Insulating Gap of UO2. *Phys. Rev. Lett.* **2002**, *89*, 266402–266404.
81. Prodan, I. D.; Sordo, J. A.; Kudin, K. N.; Scuseria, G. E.; Martin, R. L. Lattice Defects and Magnetic Ordering in Plutonium Oxides: A Hybrid Density Functional-Theory Study of Strongly Correlated Materials. *J. Chem. Phys.* **2005**, *123*, 014703-1–014703-5.
82. Prodan, I. D.; Scuseria, G. E.; Martin, R. L. Assessment of Metageneralized Gradient Approximation and Screened Coulomb Hybrid Density Functionals on Bulk Actinide Oxides. *Phys. Rev. B* **2006**, *73*, 045104-1–045104-10.
83. Hay, P. J.; Martin, R. L.; Uddin, J.; Scuseria, G. E. Theoretical Study of CeO_2 and Ce_2O_3 Using a Screened Hybrid Density Functional. *J. Chem. Phys.* **2006**, *125*, 034712-1–034712-8.
84. Kasinathan, D.; Kunes, J.; Koepernik, K.; Diaconu, C. V.; Martin, R. L.; Prodan, I. D.; Scuseria, G. E.; Spaldin, N.; Petit, L.; Schulthess, T. C.; Pickett, W. E.; et al. Mott Transition of MnO under Pressure: A Comparison of Correlated Band Theories. *Phys. Rev. B* **2006**, *74*, 195110-1–195110-12.
85. Perdew, J. P.; Burke, K.; Ernzerhof, M. Generalized Gradient Approximation Made Simple. *Phys. Rev. Lett.* **1996**, *77*, 3865–3868.
86. Rochefort, A.; Salahub, D. R.; Avouris, P. Effects of Finite Length on the Electronic Structure of Carbon Nanotubes. *J. Phys. Chem. B* **1999**, *103*, 641–646.
87. Frisch, M. J. *GAUSSIAN Development Version*, revision F.02; Gaussian, Inc.: Wallingford, CT, 2004.
88. In order to obtain the antiferromagnetic-type ground state, we used an initial guess with broken symmetry using the Guess=Mix keyword in Gaussian. When this procedure failed to converge to the long-range AFM-type ground state, we had to prepare the initial guess in an appropriate spin alignment. This was achieved by using the converged results of a higher spin multiplicity state calculation with parallel spins on both edges and flipping the spins associated with the atomic orbitals on one of the edges of the CNT.
89. Heyd, J.; Scuseria, G. E.; Ernzerhof, M. Hybrid Functionals Based on a Screened Coulomb Potential. *J. Chem. Phys.* **2003**, *118*, 8207–8215.
90. Heyd, J.; Scuseria, G. E.; Ernzerhof, M. Erratum: Hybrid Functionals Based on a Screened Coulomb Potential. [*J. Chem. Phys. 118*, 8207 (**2003**)]; *J. Chem. Phys.* **2006**, *124*, 219906.
91. Izmaylov, A. F.; Scuseria, G. E.; Frisch, M. J. Efficient Evaluation of Short-Range Hartree−Fock Exchange in Large Molecules and Periodic Systems. *J. Chem. Phys.* **2006**, *125*, 104103-1–104103-8.
92. Heyd, J.; Scuseria, G. E. Efficient Hybrid Density Functional Calculations in Solids: Assessment of the Heyd−Scuseria−Ernzerhof Screened Coulomb Hybrid Functional. *J. Chem. Phys.* **2004**, *121*, 1187–1192.
93. Heyd, J.; Peralta, J. E.; Scuseria, G. E. Energy Band Gaps and Lattice Parameters Evaluated with the Heyd−Scuseria−Ernzerhof Screened Hybrid Functional. *J. Chem. Phys.* **2005**, *123*, 174101-1–174101-8.
94. Brothers, E. N.; Izmaylov, A. F.; Normand, J. O.; Barone, V.; Scuseria, G. E. Accurate Solid-State Band Gaps *via* Screened Hybrid Electronic Structure Calculations. *J. Chem. Phys.* **2008**, *129*, 011102-1–011102-4.
95. Barone, V.; Peralta, J. E.; Wert, M.; Heyd, J.; Scuseria, G. E. Density Functional Theory Study of Optical Transitions in Semiconducting Single-Walled Carbon Nanotubes. *Nano Lett.* **2005**, *5*, 1621–1624.
96. Barone, V.; Peralta, J. E.; Scuseria, G. E. Optical Transitions in Metallic Single-Walled Carbon Nanotubes. *Nano Lett.* **2005**, *5*, 1830–1833.
97. Barone, V.; Hod, O.; Scuseria, G. E. Electronic Structure and Stability of Semiconducting Graphene Nanoribbons. *Nano Lett.* **2006**, *6*, 2748–2754.
98. Hariharan, P. C.; Pople, J. A. The Influence of Polarization Functions on Molecular Orbital Hydrogenation Energies. *Theor. Chim. Acta* **1973**, *28*, 213–222.